

Research Paper

At the same age, metallicity, and alpha-enhancement, sodium is a more effective tracer of the young and old sequences of the Milky Way disc

Evans K. Owusu^{1,3}, Sven Buder^{2,3}, Ashley J. Ruiter^{1,3,4}, Ivo R. Seitenzahl¹ and Nicolas Rodriguez-Segovia¹

¹School of Science, University of New South Wales Canberra, Australia Defence Force Academy, ACT 2600, Australia

²Research School of Astronomy and Astrophysics, Australian National University, ACT 2611, Australia

³ARC Centre of Excellence for All-Sky Astrophysics in 3 Dimensions (ASTRO-3D)

⁴OzGrav: The ARC Centre of Excellence for Gravitational Wave Discovery, Hawthorn, VIC 3122, Australia

Abstract

Trends in the enrichment of elements with stellar ages are a powerful avenue to identify unexplained origins of the elements. We investigate the stellar abundance trends of low to intermediate-mass stars using the GALAH DR3 high-resolution spectroscopic dataset of 6234 solar-type stars. Our study explores the elemental abundance $[X/Fe]$ of sodium (Na) with age. We find a pronounced enrichment in $[Na/Fe]$ at super solar metallicity (i.e., $[Fe/H] > 0$) in the old sequence of Milky Way disc stars, a trend demanding a deeper understanding of the underlying source(s) responsible for the nucleosynthesis. This progressive $[Na/Fe]$ enrichment at the young end of the old sequence has essential implications for Galactic archaeology. In this work, we propose a novel selection technique for separating the Milky Way's thick and thin disc stellar populations (i.e., old and young sequences) based on the observed $[Na/Fe]$ rise of ~ 0.1 dex for stars around 5 – 8 Gyr old. We also compare our selection method to the conventional $[Mg/Fe]$ vs $[Fe/H]$ selection approach, and we find that our new Na-based selection method better disentangles the overlap between young- and old-sequence disc stars at these intermediate ages. This is especially true at super solar $[Fe/H]$, where $[Mg/Fe]$ vs $[Fe/H]$ or $[\alpha/Fe]$ vs $[Fe/H]$ separation approaches exhibit a lot of overlap. This new selection method should help us better understand the Milky Way disc's formation history.

Keywords: Galaxy: abundances – Galaxy: evolution – Stars: abundances – Nucleosynthesis

(Received 30 04 2024; revised xx xx xxxx; accepted xx xx xxxx)

1. Introduction

Understanding the origin of the elements is a long-standing, unresolved fundamental problem of astrophysics. Numerous works over the last several decades have focused on understanding the production sites (Burbidge et al. 1957; Timmes et al. 1995; José & Iliadis 2011; Kobayashi et al. 2020, to name a few). Extensive modern spectroscopic surveys like the Galactic Archaeology with HERMES survey (GALAH, De Silva et al. 2015; Buder et al. 2018, 2021), provide a chance to advance our knowledge of the synthesis and enrichment of elements in the Milky Way and its satellite galaxies through the measurement of chemical abundances for about 30 elements in hundreds of thousands of stars. These surveys give us the capability to observe a large number of stars that cover a wide range of Galactic environments, i.e., the Milky Way's stellar halo, bulge and discs, and in some cases, even stars that were born outside of our Milky Way (e.g. Buder et al. 2022). Their uniform data acquisition also enables uniform data reduction and analysis, thus reducing systematic uncertainties. Such stellar abundance data sets are ideal for evaluating theoretical stellar nucleosynthesis models.

Of the many elements covered by the GALAH survey, we focus in this paper mostly on sodium (Na), an odd-Z element with only

one stable isotope, ^{23}Na , which has 11 protons and 12 neutrons in its nucleus. In the low-metallicity regime ($-3.0 \leq [Fe/H] \leq -1$), Na is diagnostic of a star's birthplace in terms of whether it was born inside or outside of the Milky Way (Nissen & Schuster 2010; Smiljanic et al. 2016; Das et al. 2020; Buder et al. 2022; Lombardo et al. 2022). However, the diagnostic potential of Na has not been tested extensively in the metal-rich regime (i.e., above solar metallicity), although the data show promising possibilities. It was noted already over 40 years ago that the abundance of Na relative to Fe tended to decrease toward low metallicities (Peterson 1981). We notice that in the pioneering papers by Bensby et al. (2014), Nissen et al. (2020) and Griffith et al. (2022), the Na abundance increases much above the solar ratio for stars with super-solar metallicity (Bensby et al. 2017). This is interesting because this metal-rich regime is populated by stars of the young, dynamically cold and thus thin stellar disc and the old, dynamically hotter and thick stellar disc. After the first identification of two disc populations in our Milky Way's stellar disc by Yoshii (1982) and Gilmore & Reid (1983), considerable effort has been put into studying the overlap of these populations (e.g. Bensby et al. 2014; Buder et al. 2019; Nissen et al. 2020). Until now, no simple, simultaneously observationally- and computationally economical way to separate the stars of these two-disc populations without contamination has thus far been identified.

Nissen et al. (2020) extended earlier high-precision investigations of elemental abundances in solar twin stars (e.g. da Silva

Author for correspondence: E. K. Owusu, Email: e.owusu@unsw.edu.au
Cite this article: Owusu et al. 2024, PASA, submitted.

et al. 2012; Nissen 2015; Spina et al. 2018; Bedell et al. 2018) to a more extensive metallicity range to examine how $[\text{Fe}/\text{H}]$ influences trends in elemental ratios with stellar age. To determine the ages of 72 nearby solar-type stars with metallicities in the range of $-0.3 \leq [\text{Fe}/\text{H}] \leq 0.3$, Nissen et al. (2020) analysed High Accuracy Radial velocity Planet Searcher (HARPS) spectra with signal-to-noise ratios $S/N \geq 600$ at $\lambda \sim 6000 \text{ \AA}$. The Århus STellar Evolution Code (ASTEC; Christensen-Dalsgaard 2008) stellar models were used to determine heavy element abundances, stellar ages from effective temperatures, and luminosities obtained via Gaia DR2 parallax. From their study, the age and metallicity distribution is as follows: Two different populations were distinguished, namely: an older sequence of stars with a high rise in $[\text{Fe}/\text{H}]$ to $+0.3$ dex at the age of 7 Gyr and a younger sequence with an increase in $[\text{Fe}/\text{H}]$ from -0.3 dex to $+0.2$ dex during the previous 6 Gyr (see their figures 3 and 4). Additionally, as a function of stellar age, the trends of some abundance ratios, including $[\text{O}/\text{Fe}]$, $[\text{Na}/\text{Fe}]$, $[\text{Ca}/\text{Fe}]$, and $[\text{Ni}/\text{Fe}]$, are divided into two corresponding sequences. On the other hand, the $[\text{Y}/\text{Mg}]$ -age relation exhibits no offset between the two age sequences and has no appreciable dependence on $[\text{Fe}/\text{H}]$. More striking, the age-metallicity distribution being split into two sequences indicates two instances of gas accretion onto the galactic disc with a quenching of star formation in between. Hereafter, we will follow the notation of Nissen et al. (2020) and refer to the old high-alpha, thick disc as the "old sequence" and the young low-alpha, thin disc as the "young sequence".

In a study exploring the solar neighbourhood model, Kobayashi et al. (2011) found that there was an overproduction of $[\text{Na}/\text{Fe}]$ ($[\text{Na}/\text{Fe}] \sim 0.3$ dex). However, this issue was resolved in a subsequent study by Kobayashi et al. (2020), which used updated reaction rates and considered non-local thermodynamic equilibrium (NLTE) factors that cause variation towards higher metallicities. The decrease in $[\text{Na}/\text{Fe}]$ occurs due to Type Ia supernovae, which produce more Fe than Na. Nevertheless, high metallicities were observed to show adequate Na abundances (Andrievsky et al. 2011; Zhao et al. 2012).

Among α -elements, Ca is under-abundant relative to the other α -elements in elliptical galaxies (Kobayashi et al. 2011). However, a recent study by Cinquegrana & Karakas (2022) predicts an upturn for Na yields at higher metallicities (see Fig. 4, bottom right-hand panel). The increase in Na is attributed to the competition between the production of ^{23}Na via the Ne–Na chain and the two main destruction channels: $^{23}\text{Na}(p, \alpha)^{20}\text{Ne}$ and $^{23}\text{Na}(p, \gamma)^{24}\text{Mg}$. These reactions depend heavily on the temperature in the stellar envelope and the extent of the burning. Although the intermediate-mass models endure Hot Bottom Burning (HBB), none reach temperatures capable of activating the Ne–Na chain until $M \geq 7 M_{\odot}$. As a result, the ^{23}Na surface abundance also increases during the second dredge-up (SDU), which occurs consistently with the increased sodium for the range of metallicities studied.

In this paper, we show that the observed upturn (enrichment) of Na abundance in the metal-rich regimes, that is $[\text{Fe}/\text{H}]_{\odot} > 0$, appears to be a unique characteristic of the older stellar disc, which allows for a separation method yielding a less-contaminated sampling of the thin and thick disc. If such a selection is reasonable, one could more efficiently study the stellar populations of the discs when they otherwise overlap in many characteristics like age, metallicity, alpha-enhancement and dynamics. To this end, we use the third data release of the GALAH Survey (Buder et al. 2021), which provides us with stellar chemical abundances and isochrone

interpolated ages through the overlap with the *Gaia* satellite (Gaia Collaboration et al. 2021).

The following issues are explored in this study:

- We report the $[\text{Na}/\text{Fe}]$ overproduction in GALAH DR3 at $[\text{Fe}/\text{H}]_{\odot} > 0$ and highlight possible reasons for it. We additionally carry out a brief discussion of several other elements in the context of nucleosynthesis and Galactic enrichment.
- We analyse how much our proposed new selection criteria improve the old and young sequence selection.

In Section 2, we detail our data, selection criteria, and methodology for obtaining abundances in GALAH DR3. We also describe the age determination using the BSTEP method and explore various Galactic components. In Section 3, we highlight the results from our work and Section 4 delves into a discussion of the findings and their implications. Finally, in Section 5, we offer some perspectives for future research.

2. Data

2.1. The GALAH Survey

The third data release (DR3) of the GALactic Archaeology with High Efficiency and Resolution Multi-Element Spectrograph (HERMES; at the Anglo-Australian Telescope)(Sheinis et al. 2015), hereafter GALAH, is a high-resolution ($R \sim 28000$) spectroscopic sample of stars in the Milky Way Galaxy that offers atmospheric parameters and abundances for 30 elements for almost 600 000 stars (Buder et al. 2021). GALAH is, therefore, another extensive stellar spectroscopic survey like SEGUE (Yanny et al. 2009), RAVE (Kordopatis et al. 2013), and APOGEE (Anders et al. 2014). These surveys serve as a window to study the formation and evolutionary history of our Galaxy and astrophysical processes that have occurred using traces of gas that have been transported and incorporated into the formation of new generations of stars throughout history. Primarily, GALAH targets relatively bright stars in the magnitude range of $9 < V < 14$, which are therefore mostly nearby, typically closer than 2 kpc. In GALAH DR3, up to 30 elemental abundances are provided, along with their uncertainties, quality flags, surface gravity, effective temperatures, and ages. The ages were determined using the Bayesian stellar parameter estimation code (BSTEP; Sharma et al. 2018).

2.2. Abundances and how they are determined in GALAH DR3

GALAH DR3 provides analyses of stellar spectra from the HERMES spectrograph, which covers four wavelength bands in the optical and near-infrared ($4713 - 4903$, $5648 - 5873$, $6478 - 6737$, and $7585 - 7887 \text{ \AA}$) (Sheinis et al. 2015). The abundances of up to 30 elements were derived using the 1D MARCS model atmospheres (Gustafsson et al. 2008), and a modified version of the Spectroscopy Made Easy (SME) spectrum synthesis code (Valenti & Piskunov 1996; Piskunov & Valenti 2017). Of these elements, 11 were computed using non-local thermodynamic equilibrium (NLTE; Amarsi et al. 2020) and the remaining 19 elements were determined using local thermodynamic equilibrium (LTE). The abundance analysis is preceded by a step that derives the global stellar parameters from the spectra, namely effective temperature (T_{eff}), surface gravity ($\log g$), iron abundance $[\text{Fe}/\text{H}]$, micro-turbulence velocity (v_{mic}), broadening velocity (v_{broad}) and

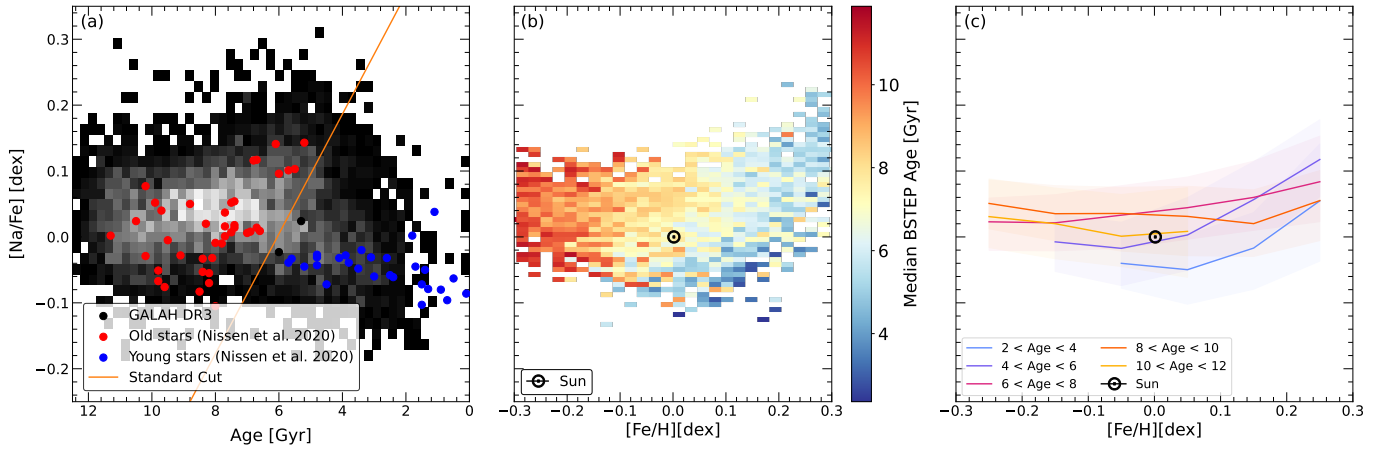


Figure 1. Different representations of the age-iron-sodium abundance relations for solar-type stars of Nissen et al. (2020) and GALAH DR3 (selected via Eq. 5). Panel (a) shows age vs. $[\text{Na}/\text{Fe}]$ measurements by Nissen et al. (2020) with old (red) and young (blue) sequences. The density distribution of GALAH DR3 solar-type stars is shown in greyscale in the background. Panel (b) shows the 2-dimensional distribution of $[\text{Na}/\text{Fe}]$ vs $[\text{Fe}/\text{H}]$ of the GALAH DR3 solar-type stars coloured by median age, with the Sun indicated via \odot . Panel (c) shows the same plane but with the distribution of $[\text{Na}/\text{Fe}]$ in 2 Gyr age bins for 0.1 dex $[\text{Fe}/\text{H}]$ bins. The lines represent the median, whereas the contours show the 16th to 84th percentiles.

radial velocity (v_{rad}). For ease, the elemental abundances as logarithmic ratios of number densities N , that is,

$$[A/B] \equiv \log_{10}(N_A/N_B)_* - \log_{10}(N_A/N_B)_\odot \quad (1)$$

for two elements A and B, are normalised to iron and the solar values (\odot), and abundances are reported as $[X/\text{Fe}] = [X/\text{H}] - [\text{Fe}/\text{H}]$.

The ages of stars in GALAH DR3 were computed using a Bayesian Scheme known as the Bayesian Stellar Parameters estimator (BSTEP Sharma et al. 2018) with an elaborate step-by-step distribution given in section 3 of Sharma et al. (2018).

2.3. Sample Selection

To assess the nature of the abundance enrichment and its correlation with stellar age, we apply an overall quality cut and then divide the overall data set into a smaller sample of solar-type stars, which are cool main-sequence dwarfs located below the red edge of the classical instability strip (spectral types from late F, G and K dwarfs, Soderblom & King 1998; García & Ballot 2019).

For this study, we apply the following quality cuts:

$$\text{flag_sp} == 0, \text{flag_fe_h} == 0, \text{flag_Na_fe} == 0, \quad (2)$$

$$\text{e_age_bstep}/\text{age_bstep} < 0.2 \text{ or } \text{e_age_bstep} < 2, \quad (3)$$

$$\text{snr_c2_iraf} > 50, \quad (4)$$

$$5600 < T_{\text{eff}} < 5950, \log g > 4.15, \text{ and } -0.3 < [\text{Fe}/\text{H}] < 0.3 \quad (5)$$

We employ basic quality cuts to select only unflagged measurements (Eq. 2). Because our study relies on reasonably determined ages, we further limit our sample to stars with either less than 20% age uncertainty or age uncertainties below 2 Gyr (Eq. 3). To ensure a reasonable quality of measurements, we set a lower spectrum quality cut of signal-to-noise in the green CCD of 50 per pixel (Eq. 4). We further limit our sample to solar-type stars via Eq. 5, following the definition of Nissen et al. (2020).

Whenever we use elemental abundances $[X/\text{Fe}]$, we further apply a quality cut of

$$\text{flag_X_fe} == 0. \quad (6)$$

X replaces the respective element, e.g. Na, for good sodium measurements.

3. Analysis

The motivation for this project is the Nissen et al. (2020) age-metallicity separation (see their figs. 3 and 4) of old and young solar-type stars, which were historically equated as thick and thin disc sequences, respectively. The upturn in $[\text{Na}/\text{Fe}]$ with age for the old solar-type stars in their measurements especially caught our eye. We reproduce this plot in Fig. 1a and also identify an upturn of Na in the $[\text{Na}/\text{Fe}]$ vs $[\text{Fe}/\text{H}]$ (Fig. 1b) and $[\text{Fe}/\text{H}]$ versus $[\text{Na}/\text{Fe}]$ relationship with age bin in step size of 2 Gyr (see Fig. 1c) for $[\text{Fe}/\text{H}]_\odot > 0$ in the GALAH data. In Fig. 1b), the standard deviation of the ages for stars around solar metallicity is ± 2 Gyr.

Our analysis, therefore, first focuses on the dissection of the upturn of $[\text{Na}/\text{Fe}]$ at iron abundances above $[\text{Fe}/\text{H}] > 0$ in Sec. 3.1. We then show that increasing $[\text{Na}/\text{Fe}]$ vs age can improve the selection of co-natal young and old sequence stars in Sec. 3.2. In Sec. 3.3, we then assess the trends of young and old sequences in the other age-abundance planes available with GALAH DR3 data before confirming the robustness of our selection function in Sec. 3.4.

3.1. The upturn of $[\text{Na}/\text{Fe}]$ at $[\text{Fe}/\text{H}] > 0$

We show the $[\text{Na}/\text{Fe}]$ versus $[\text{Fe}/\text{H}]$ relation with bin median ages in a step size of 2 Gyr (see Fig. 1c). The important observation takeaway is that for all the age bins explored in this work, ages between 2 – 6 Gyr for $[\text{Na}/\text{Fe}]$ are more enriched; the abundance rises from solar value to 0.12 dex followed by 6 - 8 Gyr, which are stars mostly confined to the thick disc. The resulting differences in $[\text{Na}/\text{Fe}]$ enhancement for different ages motivated us to test its potential to separate stars of the young and old sequence of the Milky Way disc.

3.2. Selecting young and old stars in the $[\text{Na}/\text{Fe}]$ -Age plane

The Milky Way's stellar disc is a complex structure, and its formation and evolution are still widely debated (e.g. Katz et al. 2021). Several surveys have provided large statistical samples of stars with detailed chemical abundances, such as RAVE (Kunder et al.

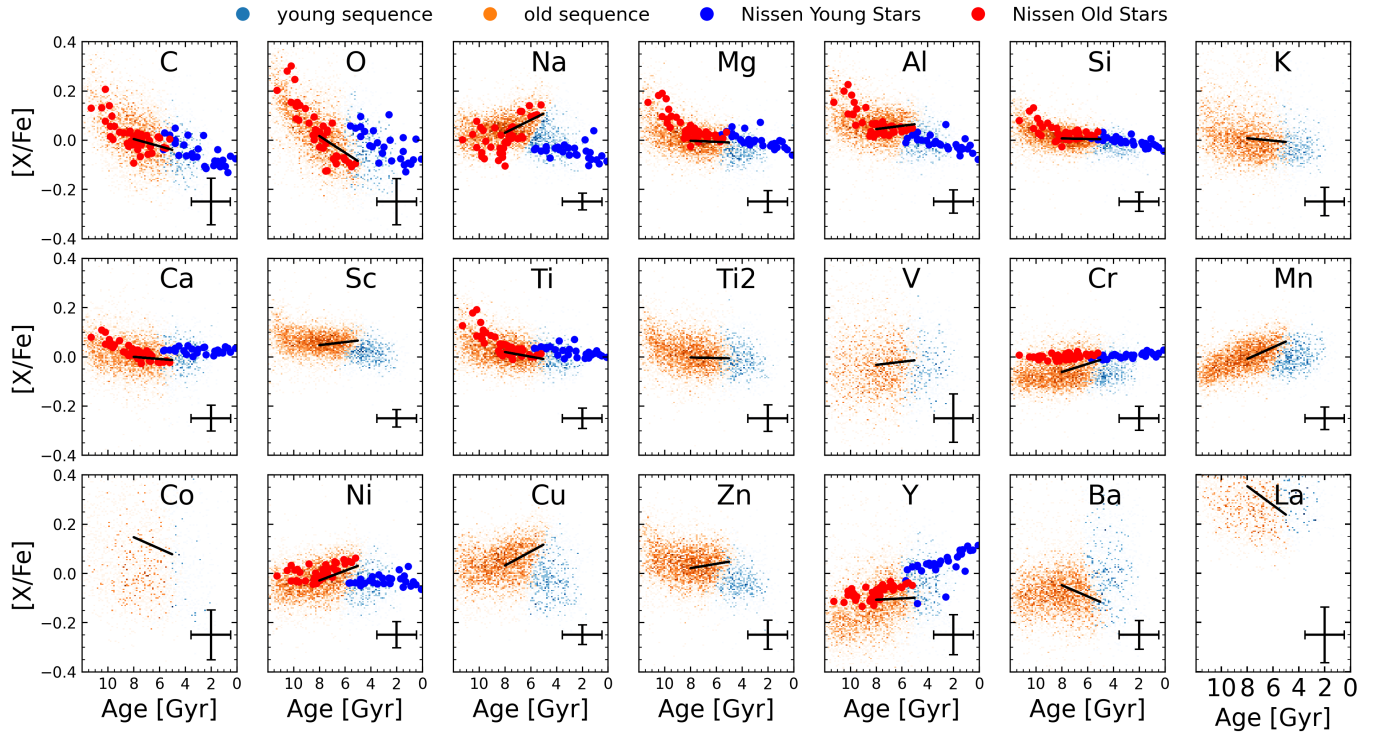


Figure 2. Age-abundance distributions of young and old solar-type stars for the elements measured by GALAH DR3 (small dots in the background) and Nissen et al. (2020, larger dots in foreground). Reddish colours represent stars of the old sequence and blueish colours represent stars of the young sequence, respectively, as selected via Eq. 5. The elements are indicated in each panel. The black lines indicate a linear fit to the old sequence of GALAH DR3 between 5 and 8 Gyr. Typical uncertainties in this age range are shown as error bars in the bottom right.

2017), Gaia-ESO (Randich et al. 2013), APOGEE (Alam et al. 2015), LAMOST (Zhao et al. 2012) and GALAH (Buder et al. 2018), combined with very precise Gaia astrometry (Lindegren et al. 2018), making it possible to examine the formation of the Galactic disc with an unprecedented level of detail. The sample includes mainly thin and thick disc stars of all ages selected based on various criteria, such as the relative abundance of alpha-elements and stellar ages within the old sequence of the Milky Way disc. Due to the overlap of the thin and thick disc stars, several studies (see for instance Lee et al. 2011; Delgado Mena et al. 2021; Bensby et al. 2014; Recio-Blanco et al. 2014; Hayden et al. 2017) have come up with preliminary techniques to separate the contamination of the two-disc sequences. However, kinematics and chemo-dynamics have proven not to be accurate in distinguishing both sequences, especially at intermediate ages (Hayden et al. 2017) in the metallicity range of -0.3 to $+0.5$ dex, where both sequences overlap (e.g. Bensby et al. 2014).

We continue our analysis by reproducing the selection of young and old sequences in the age-abundance plane similar to Nissen et al. (2020). However, contrary to Nissen et al. (2020), who use a selection in the age vs. $[\text{Fe}/\text{H}]$ space, we select stars via age and $[\text{Na}/\text{Fe}]$. Thick and thin solar-type stars from the study of Nissen et al. (2020) (old thick disc stars in red and young thin disc stars in royal blue) are superimposed over the GALAH DR3 solar-type stars data (shown in grey, see Fig. 1).

Fig 1a, in particular, shows an initial selection (hereafter standard cut) based on a separation ‘by eye’ of the Nissen et al. (2020)-stars as an orange line. We classify stars as young or old, whether they are below or above the line as:

$$\left. \begin{aligned} \text{old stars : } & [\text{Na}/\text{Fe}]_{\text{old}} > 0.55 - 0.5/5.5 \times \tau \\ \text{young stars : } & [\text{Na}/\text{Fe}]_{\text{young}} < 0.55 - 0.5/5.5 \times \tau \end{aligned} \right\}, \quad (7)$$

Where τ represents the stellar age, we discuss the sensitivity of our results to variations of our standard cut in Sec. 3.4 to test the robustness of our selection criteria for the GALAH data sample. For Nissen et al. (2020), this cut is robust mainly due to the difference of $[\text{Na}/\text{Fe}]$ rise of ~ 0.30 dex around 5 Gyr.

Our selection now allows us to assess the age-abundance distribution for all other elements in Fig. 2, which shows the solar-type thick (red colour) and thin (royal blue colour) disc stars from Nissen et al. (2020) overlaid on GALAH DR3 solar-type thick (orange) and thin disc (sky blue) stars respectively.

While we have established the clear upturn of $[\text{Na}/\text{Fe}]$ for the old sequence, the trends for other elements are more diverse. While other odd-Z elements like aluminium (Al) and scandium (Sc) also demonstrate a rise in their abundance with decreasing stellar age, their rise is less pronounced than that of sodium. When we consider potassium (K), another odd-Z element, it shows a unique trend (i.e., it remains flat), though we note K is less well-constrained in the $[\text{X}/\text{Fe}]$ axis. Furthermore, alpha elements (i.e., C, O, Si, Ca and Mg) show decreasing trends. On the other hand, elements near the iron peak (i.e., Cr, Mn, Ni, Cu, Co and Zn) demonstrate increasing upward trends. More so, the neutron capture element yttrium (Y) remains flat, while barium (Ba) shows a decreasing trend. Section 4.2 discusses possible underlying reasons for these trends.

3.3. Quantifying Age-Abundance Trends

Next, we test how robust our age-abundance trends are regarding the particular selection function (cut) chosen in the $[\text{Na}/\text{Fe}]$ -age plane.

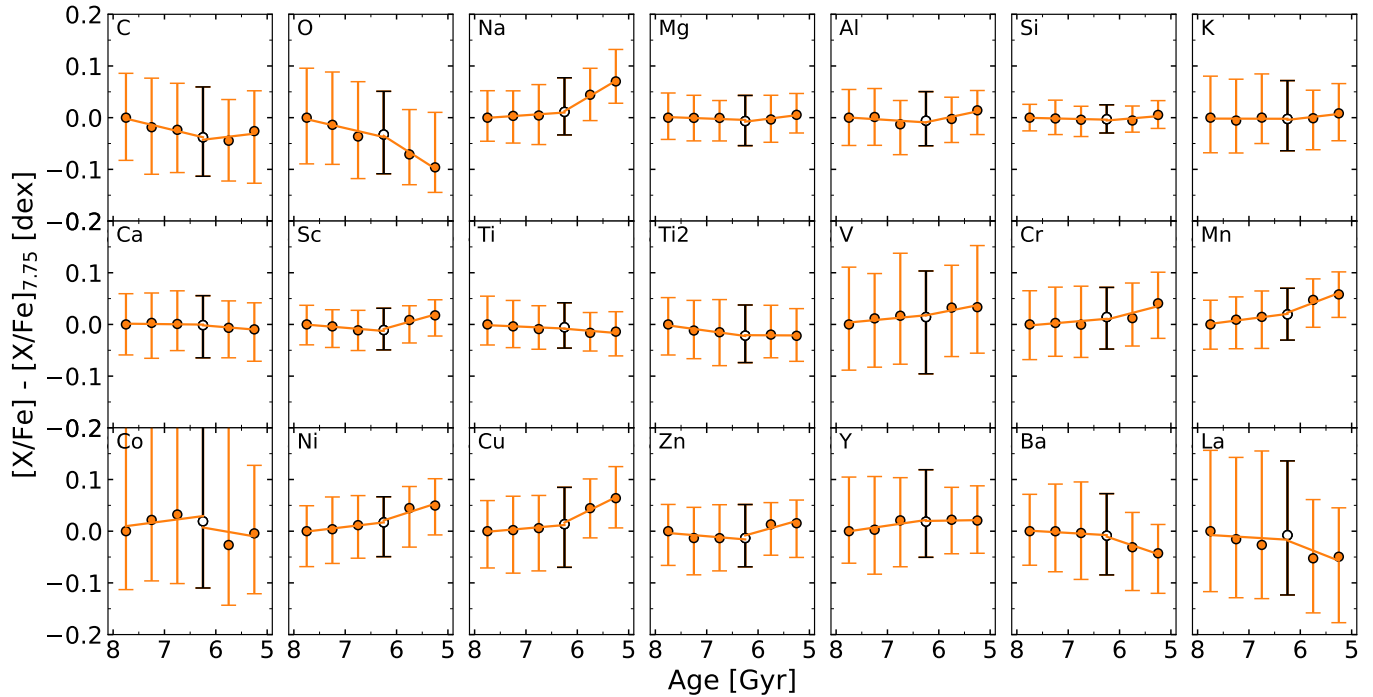


Figure 3. Age-abundance distributions and fits these distributions of the old solar-type stars between 5 and 8 Gyr as measured by GALAH DR3. Each panel shows median abundances within 0.5 Gyr bins as dots for the element in the top left. Error bars represent each bin's spread between the 16th and 84th percentile. To allow a better comparison of trends across all considered elements, the abundances have been artificially shifted for Fig. 2 so that all bins of the oldest stars (~ 7.85 Gyr) have Solar abundance. In addition to a linear fit to the full age range (from 5 to 8 Gyr), we performed linear fits to the stars above and below 6.3 Gyr, with gradients of $\Delta[X/Fe]/\text{Gyr}$. While this figure shows the binned data, the fits were performed on the sets of individual stars. We show the result of the fits in Tab. 1.

Table 1. Gradient estimates for the age-abundance trends for elements of the old solar-type stars of GALAH DR3 between 5 and 8 Gyr. We report both median slopes between 5 and 8 Gyr as well as those for intervals of 5 – 6.5 Gyr and 6.5 – 8 Gyr.

Atomic Number	Element	Gradient 5.0 – 8.0 Gyr dex Gyr ⁻¹	Gradient 6.5 – 8.0 Gyr dex Gyr ⁻¹	Gradient 5.0 – 6.5 Gyr dex Gyr ⁻¹
6	C	-0.0145 ± 0.0024	-0.0125 ± 0.0053	-0.0199 ± 0.0078
8	O	-0.0339 ± 0.0025	-0.0210 ± 0.0056	-0.0652 ± 0.0084
11	Na	0.0260 ± 0.0009	0.0066 ± 0.0021	0.0673 ± 0.0031
12	Mg	-0.0022 ± 0.0012	-0.0090 ± 0.0027	0.0119 ± 0.0041
13	Al	0.0066 ± 0.0012	-0.0113 ± 0.0027	0.0263 ± 0.0041
14	Si	-0.0011 ± 0.0011	-0.0068 ± 0.0024	0.0053 ± 0.0035
19	K	-0.0051 ± 0.0016	-0.0058 ± 0.0035	0.0021 ± 0.0053
20	Ca	-0.0043 ± 0.0014	-0.0017 ± 0.0031	-0.0059 ± 0.0046
21	Sc	0.0062 ± 0.0009	-0.0052 ± 0.0021	0.0256 ± 0.0031
22	Ti	-0.0095 ± 0.0011	-0.0103 ± 0.0024	-0.0144 ± 0.0035
22	Ti2	-0.0011 ± 0.0012	-0.0054 ± 0.0029	0.0065 ± 0.0037
24	V	0.0063 ± 0.0027	-0.0019 ± 0.0062	0.0292 ± 0.0094
25	Cr	0.0164 ± 0.0013	0.0092 ± 0.0029	0.0388 ± 0.0043
27	Mn	0.0236 ± 0.0012	0.0137 ± 0.0027	0.0516 ± 0.0041
28	Co	-0.0230 ± 0.0031	0.0544 ± 0.0077	-0.0698 ± 0.0099
29	Ni	0.0199 ± 0.0013	0.0064 ± 0.0029	0.0433 ± 0.0043
30	Cu	0.0285 ± 0.0010	0.0080 ± 0.0023	0.0723 ± 0.0034
39	Zn	0.0092 ± 0.0015	-0.0076 ± 0.0034	0.0257 ± 0.0051
56	Y	0.0027 ± 0.0022	0.0160 ± 0.0048	-0.0262 ± 0.0071
57	Ba	-0.0226 ± 0.0016	-0.0016 ± 0.0035	-0.0652 ± 0.0052

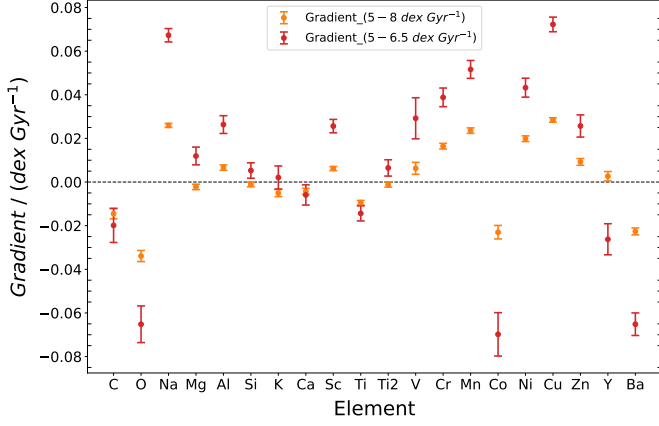


Figure 4. Gradient estimates of abundances, $\Delta[X/Fe]/\Delta\text{Age}$ of different elements X for old solar-type stars as selected with the Standard Cut from Eq. 7. Positive values indicate an increase of element X over iron with time, whereas negative values show a relative decrease in the abundance of element X relative to iron with time. Error bars indicate the fitting uncertainties. We note that most of the enrichment for intermediate mass and iron peak elements occurs between 5 and 6.5 Gyr, e.g. during the birth of stars representing the younger end of the old sequence.

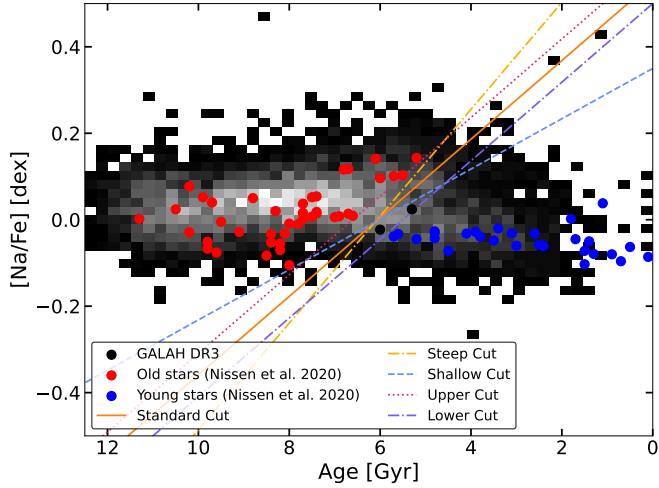


Figure 5. Similar to Fig. 1a for the entire age range considered (5-8 Gyr), but now including different cuts to separate old from young solar-type stars (see Eqs. 8-11).

3.4. How robust is the newly suggested selection via the age-[Na/Fe] plane?

To test the robustness of our [Na/Fe] versus age trend against the details of the choice of the standard cut in Eq. 7, we consider further cuts (as shown in Fig. 5) defined by the equations below:

$$\text{upper cut: } [Na/Fe] = 0.55 (-0.05) - 0.5/5.5 \times \tau, \quad (8)$$

$$\text{lower cut: } [Na/Fe] = 0.55 (+0.05) - 0.5/5.5 \times \tau, \quad (9)$$

$$\text{steep cut: } [Na/Fe] = 0.75 - 0.68/5.5 \times \tau \text{ and} \quad (10)$$

$$\text{shallow cut: } [Na/Fe] = 0.35 - 0.32/5.5 \times \tau. \quad (11)$$

The effect of these various cuts is shown in Fig. 6, where τ is the age of stars in Gyr.

From Fig. 1, we observed a [Na/Fe] enhancement of (~ 0.12) dex from approximately solar value through to high metallicity

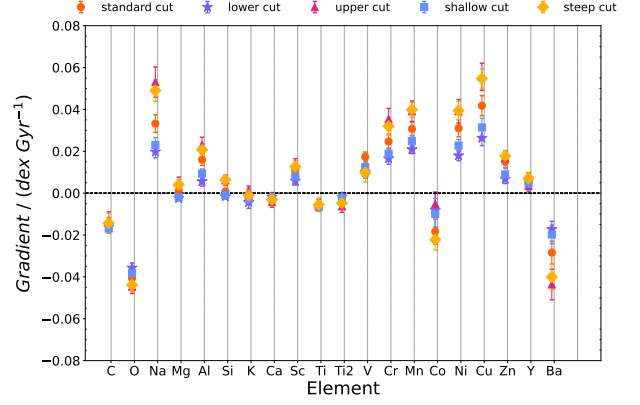


Figure 6. Gradients for the same elements as in Fig. 4, but this time, the gradient value is taken over the larger age range that is shown in Fig. 5 for the various selection cuts that are displayed. Colours correspond to those used in Fig. 5.

(see Figs. $\sim 1a$ and $1b$). Also, in Fig. 1c, we see an upturn of [Na/Fe] beyond solar metallicity.

It has been noted that cobalt (Co) has large uncertainty values because only a few lines are present in GALAH DR3. However, for all other elements, the trends obtained from different separation cuts agree with the scatter, meaning that the slopes characterise abundance relative to iron with decreasing stellar age all cluster around the same value for the various elements. This suggests that the slope estimates for different cuts of each component are in close agreement, indicating a robust selection technique for our old sequence.

4. Discussion

We have established a strong correlation [Na/Fe]-age enhancement for the old sequence of the Milky Way. We now discuss both the implications on the nucleosynthetic channels at play and what we could learn from this about the thin and thick disc. As the main feature of our analysis, we first discuss the age-abundance relation of Na (Sec. 4.1) in detail before turning to all other elements in Sec. 4.2. This will inform our discussion of the nucleosynthetic implications for the old sequence in Sec. 4.3. Having focused on the old sequence, we will then put our results into the context of the young disc in Sec. 4.4. Given the overlap of young and old discs around 6.3 Gyr, we further discuss the nature of the change in age-abundance trends for our old sequence selection in Sec. 4.5, before discussing how much the selection of the two sequences improves when including [Na/Fe] in Sec. 4.6.

4.1. The age-abundance trend of Na for the old sequence

Sodium is an odd-Z element synthesised in i.e. exploding massive stars and dying low-mass stars. In massive stars, Na is synthesised during the hydrostatic carbon burning phase Cameron (1959); Salpeter (1952); Woosley & Weaver (1995). Also, during the neon-sodium (Ne-Na) and magnesium-aluminium (Mg-Al) cycles in dying low-mass stars, Na is produced Denisenkov & Denisenkova (1990) and mixed to the surface when approaching the red giant branch phase (e.g. El Eid & Champagne 1995; Mowlavi 1999; Karakas 2010; Cinquegrana & Karakas 2022).

Owing to the diverse sources from which Na is synthesised, its abundance pattern as a function of metallicity is considered a complex one (Bedell et al. 2018). This assertion is further highlighted by Bensby et al. (2017), where, in a study conducted in the solar neighbourhood for the bulge, the trend of [Na/Fe] first increases with [Fe/H] because of the contributions from massive stars that produce Na and Fe; however when the nucleosynthetic products of SNe Ia begin to have a significant impact on a stellar population $\sim 0.4 - 1$ Gyr after star formation (Ruiter et al. 2011, see fig. 2), [Na/Fe] starts to drop with [Fe/H]. As a result, the trend of [Na/Fe] over time (i.e., metallicity and age) has been described as a “zigzag” one (McWilliam 2016). This trend is important for our consideration because the bulge shares the same abundance trend with the thin and thick disc (Bensby et al. 2017).

The study of Nissen et al. (2020) reported a rise in [Na/Fe]-age of 0.15 dex for the same stellar population at the same age range (i.e., 5 - 8 Gyr). Similarly, a linear fit to the old sequence at intermediate ages of 5 - 8 Gyr gives a gradient value of $(0.0260 \pm 0.0009 \text{ dex/Gyr})$, i.e. 0.077 dex for the stated age rang) for [Na/Fe]. Which is much lower than the value reported by Nissen et al. (2020). Also, a steeper rise for [Na/Fe] occurs between the ages of (5 - 6.5) Gyr with abundance gradient of $0.0673 \pm 0.0031 \text{ dex/Gyr}$ (see red data points in Fig 4) compared with that of $(0.0066 \pm 0.0021 \text{ dex/Gyr})$; see Tab. 1).

We indeed see an explicit knee behaviour McWilliam (2016) for several elements in our study, with a plateau behaviour for stars aged 8-6.3 Gyr followed by a change in slope – going up or down – from ages 6.3 to 5 Gyr. One may assume then that iron enrichment from SNe Ia becomes more critical around the time of the knee. We can see a drop for some elements that start to decline relative to iron as we look at younger (generally more metal-rich) stars owing to the (generally long) delay times attributed to SNe Ia (Matteucci & Brocato 1990; Ruiter et al. 2009; Maoz et al. 2012). An upward trend in [X/Fe] with decreasing age would be expected for some elements, particularly around the iron peak (i.e. Mn, which is mainly synthesised in SNe Ia arising from massive white dwarf stars Seitzenzahl et al. 2013). However, Na also shows an upward trend with decreasing age, but Na is not canonically associated with SNe Ia but more often with short-lived, massive stars. This means something is driving Na-enrichment other than simply the products of short-lived, massive stars. The knee effect we see in Na here would be consistent with Na being synthesised by SNII progenitors with a metallicity-dependent yield, i.e., the ‘metallicity effect’.

Novae, which are (recurring) thermonuclear eruptions on accreting white dwarfs, could also be considered as a plausible source of Na given their range of delay times (see fig 12, Kemp et al. 2021). However, preliminary work indicates that novae are not a leading contributor to sodium enrichment in the Galaxy above solar metallicity (A. Kemp, Private Comm. 2024).

Gas enrichment from massive stars that give rise to core-collapse supernovae likely contributes to the overall enrichment of sodium as we consider stellar populations at higher metallicity (i.e., younger ages). At higher metallicity, a star will typically have a lower electron fraction (i.e., Y_e , i.e., more neutrons available), where $(Y_e = N_p / (N_p + N_n))$. Low Y_e favours the production of odd-Z elements, such as Na, Al, or Sc. The reason why odd-Z elements can be produced in more significant (relative to their neighbouring even-Z elements) abundance as the metallicity of the progenitor increases is as follows: Many of the light odd-Z elements only have one stable isotope (e.g., ^{23}Na (11,12),

^{27}Al (13,14), ^{31}P (15,16), ^{45}Sc (21,24), etc.). These odd-Z stable isotopes are neutron-rich – the nuclei have more neutrons than protons. At low progenitor metallicity, a pre-supernova star will have Y_e very close to 0.5 in the relevant layers where explosive nucleosynthesis occurs since core helium burning produces mostly self-conjugate nuclei like ^{12}C , ^{16}O , and ^{20}Ne . However, with increasing metallicity, more C, N, and O nuclei are already present during hydrogen burning. The CNO cycle turns most of the nuclei present as CNO to ^{14}N .

Importantly, a main reaction during core helium burning then is $^{14}\text{N}(\alpha, \gamma)^{18}\text{F}(\beta^+ \nu_e)^{18}\text{O}(\alpha, \gamma)^{22}\text{Ne}$. In effect, by number, most CNO nuclei initially present are turned into ^{22}Ne , which, owing to the beta-decay of ^{18}F , is neutron-rich, with two extra neutrons. Since the relative number of protons to neutrons is largely conserved for many environments where explosive nucleosynthesis occurs, the extra neutrons available allow the more efficient nucleosynthesis of the neutron-rich odd-Z isotopes.

In contrast, alpha elements (i.e., the even-Z elements such as Mg, S, or Ca) have more stable isotopes that extend from self-conjugate stable nuclei on the alpha-chain [e.g., ^{24}Mg (12,12), ^{32}S (16,16), ^{40}Ca (20,20)] to several neutron-rich stable isotopes (e.g. ^{25}Mg , ^{26}Mg , . . . , ^{48}Ca). This means we can make stable even-Z element isotopes at high and low (no) neutron excess. Still, we can synthesise odd-Z elements more efficiently in environments with extra neutrons (which means higher metallicity). Higher progenitor metallicity here also means that the neutron-rich isotopes like ^{25}Mg of these even-Z elements are produced in greater abundance; however, this comes at the expense of the also stable ^{24}Mg and so the total production of the element Mg is hence overall less affected.

4.2. Age-abundance trends other than Na for the old sequence

4.2.1. Light elements

In the older sequence of the younger stellar population (i.e., from 6.3 Gyr), [(C, O)/Fe] has a decreasing trend with age (see Fig. 3). The carbon gradient remains relatively consistent across the different age ranges where the fits were conducted (i.e., 5 - 8, 6.5 - 8, and 5-6.5 Gyr). However, the abundance of oxygen relative to iron shows a significant change, decreasing by more than three-fold between the fits for 5 - 8 and 5 - 6.5 Gyr (see Tab. 1). This indicates that most of the decrease in oxygen abundance occurred between 6.5 and 5 Gyr, although, despite the decline, the ratio remains below the solar value.

Carbon (C) is primarily synthesised and expelled back into space by exploding massive stars and dying low-mass stars as well as during earlier stages of stellar evolution like core helium burning (CheB). The trend in [C/Fe] is mainly due to the reduced impact of SNII due to the short life-cycle of $\lesssim 10^7$ years for high-mass stars. In terms of enrichment, dying low-mass stars play a more dominant role, hence the decrease in solar value. [C/Fe] remains flat compared to other light elements (i.e., O).

Oxygen (O) enjoys the distinction as the most abundant nucleus synthesised in stars because it is the natural end product of helium burning. The majority of O is synthesised in exploding massive stars, partly in dying low-mass stars, and released by exploding white dwarfs (WD) (Timmes et al. 1995; Röpke et al. 2012). The contributions of SNe Ia and exploding WDs to the synthesis of O are relatively small compared to SNII.

Oxygen is one of the elements where the gradient of [O/Fe] vs age sharply changes around 6.5 Gyr (see Fig. 3). This is reflected in the fact that the gradient for the young end (from 5.0 to 6.5 Gyr) of the old sequence is much steeper than the gradient for the whole time window (from 5 -8 Gyr, see Fig. 4). This trend indicates a decline in oxygen over iron production within the old sequence in this time frame, perhaps due to SNe Ia producing iron peak elements in the younger generation of old disc stars. The decrease is consistent with the prevalent notion (e.g. Timmes et al. 1995) that [O/Fe] decreases with decreasing age as SNe Ia progressively becomes more dominant and becomes an essential source of iron. Also, we can see an apparent “knee” effect, which is interpreted as the accretion of gas onto the thin disc with a quenching of star formation (SFR) in between (McWilliam 1997; Nissen et al. 2020).

4.2.2. Alpha elements

Alpha-elements are thought to originate and expelled back into the interstellar medium, mostly from core-collapse supernovae. Several alpha-elements also have considerable contributions from low-mass stars. As a result, they are valuable indicators of the chemical development of the galaxy (Bensby et al. 2017). From Fig. 4, we see that the alpha (e.g., Mg, Si, Ca, and Ti) elemental abundances are flat in the 5-8 Gyr range. There is a slight “knee” for Mg and Si around 6.3 Gyr, where the gradient slightly turns upwards (see Fig. 4), and Ca remains essentially unchanged.

Magnesium (Mg) is synthesised primarily during explosive carbon-burning in exploding massive stars (Arnett 1995; Woosley & Weaver 1995) and dying low-mass stars (Thielemann et al. 2002). On average, SNI ejects about ten times as much Mg as Type Ia supernovae, and SNI also occur about five times more frequently. From Fig. 3, Mg has an initial flat plateau with a transition to an increasing trend at around 6.3 Gyr. We note that this is different from the conventional “knee” seen in the solar neighbourhood that describes a decrease of alpha/Fe with age as low mass stars (mostly via Fe-group producing thermonuclear supernovae) begin to modify the abundance trends (e.g. Bensby et al. 2017). Notably, if anything, we see a slight increase in [Mg/Fe] in the old sequence around 6.3 Gyr towards younger stars. The conventional wisdom is that SNe Ia produces sub-solar [Mg/Fe] (e.g. Timmes et al. 1995; Seitzzahl et al. 2013; Lach et al. 2020), making this upward trend difficult to explain with an increasing contribution from thermonuclear supernovae.

Silicon (Si) exists primarily due to oxygen-burning (Woosley 1986). Simply put, two ^{16}O nuclei collide, causing the reaction $^{16}\text{O} + ^{16}\text{O} \rightarrow ^{28}\text{Si} + ^4\text{He}$. In addition, some Si is synthesised in exploding WDs and dying low-mass stars (Matteucci & Greggio 1986; Timmes et al. 1995). We see that Si is relatively flat like Ti and other alpha process elements (e.g., Mg, Ca) with a slight increase in abundance at 6.3 Gyr (see Tab. 1; Fig. 4). Also, the trend in the older sequence of the younger stellar population (i.e., from 6.3 Gyr) for [Si/Fe] slightly increases with age. The discontinuity occurring at ~ 6.3 Gyr could be indicative of a different star formation rate, or gas accretion/enrichment phase, between the old and young sequence discs (McWilliam 1997; Nissen et al. 2020).

Calcium (Ca) is primarily synthesised owing to oxygen-and silicon-burning processes (both explosive and non-explosive) in massive stars (Timmes et al. 1995). The age vs. abundance trend for Ca across all ages remains the same.

Titanium (Ti) is primarily synthesised through the alpha-rich freezeout in core-collapse supernovae and explosive helium burning processes (i.e. Tur et al. 2010; Kromer et al. 2010; Crocker et al. 2017). In GALAH DR3, Ti2 is the ionised Ti line (all other alpha-elements are measured from their neutral lines). Table 1 lists the gradients for the age-abundance trend for titanium. The age-abundance trend for Ti remains flat in the old sequence.

4.2.3. Odd-Z elements

Odd-Z elements (Na, Al, K and Sc) provide crucial information about nucleosynthetic processes and chemical evolution in the early Galaxy. When non-LTE effects are considered, abundance trends for odd-Z elements display different trends when compared to the case when NLTE effects are not taken into account (Cayrel et al. 2004; Bandyopadhyay et al. 2020). The age-abundance trend of the younger populations (from 6.3 Gyr) of the old sequence for the odd-Z elements increases more than other elements, with Na having the most pronounced rise.

Aluminium (Al) is mainly synthesised during carbon-neon (C-Ne) burning in massive stars and the magnesium-aluminium (Mg-Al) cycle in massive AGB stars (i.e., 9 -12 M_{\odot} ; Siess 2006; Karakas 2010). The gradient of Al for the younger population (5–6.5) Gyr of the older sequence is approximately four times steeper than the trend for the old sequence (5 - 8) Gyr.

More so, even though Al is an odd-Z element, we found a behavioural trend similar to most α -elements, i.e., a plateau between 6.5-8 Gyr before an increase that gives rise to a visible “knee” effect at ~ 6.3 Gyr. An Al-enhancement at younger stellar ages has been noted in previous studies for stars in the bulge by Bensby et al. (2014, 2017).

Potassium (K) is primarily synthesised during the burning of oxygen in massive stellar explosions (Woosley & Weaver 1995; Timmes et al. 1995; Cayrel et al. 2004). K exhibits a flat plateau trend compared to other odd-Z elements (Na, Al, and Sc). Still, again, we caution that uncertainty values are relatively high for potassium, particularly at young stellar ages (see Tab. 1).

The different production sites for K compared with Na and Al could contribute to the observed trend difference.

Scandium (Sc) The two main nucleosynthesis processes in Type II supernovae that produce scandium are oxygen-burning and the alpha-rich freeze-out reassembly of alpha particles close to the collapsed core, which is the same zone where titanium is synthesised (Nakamura et al. 1999; Kobayashi et al. 2011). Factors such as stellar rotation (Prantzos et al. 2018) and two-dimensional (2D) jet-induced supernovae Kobayashi et al. (2020) can lead to increased production of Sc. On the other hand, at all metallicities, Sc is under-produced when theoretical models are compared to observations (Kobayashi et al. 2006). The gradient shows a clear increase as we go to younger stellar ages (e.g. see Tab.1).

4.2.4. Elements near the iron peak

Elements near the iron peak (V, Cr, Mn, Ni, Cu and Zn) follow the expected predictions from nucleosynthesis in that their abundance increases over time due to the increasingly important role of SNe Ia, which produce large amounts of these elements (in addition to iron) compared to other sources. From Fig. 3, an “elbow” effect, having the opposite trend as a knee effect, is

apparent, which could indicate the onset of different star formation rates between the old and young sequences. Such an effect is seen around 6.3 Gyr for the following elements: Cr, Mn, Ni, Cu and Zn. Co shows an opposite, “knee-like” trend (though we note the cobalt data has comparatively large errors, so we are currently unable to quantify the validity of this apparent trend). While Cr, Mn and Ni (and also V) show a somewhat steady increase in abundance toward younger ages, Cu and Zn exhibit the most prominent elbow effect, where the behaviour from near-flat to strongly increasing abundance is quite clear.

Vanadium (V) : V is produced both in massive stellar explosions (Weaver & Woosley 1978) and thermonuclear SNe (Seitenzahl & Pakmor 2023). V’s most abundant stable isotope is ^{51}V , with one dominant source plausibly being helium-shell detonations in sub-Chandrasekhar mass white dwarf SNe Ia (Timmes et al. 1995, see also Panther et al. (2021) for future prospects on detection of V lines in double-detonation SNe Ia). Taken over the entire age range considered for the old disc (5 - 8 Gyr), the V abundance steadily increases; however, upon closer inspection, we can see that the gradient over the younger part of the range (5 - 6.5 Gyr) is quite a bit steeper (see Tab. 1). Also, the younger population of the old sequence has a gradient variation of a factor of 2, although with a relatively more significant uncertainty. The factor of 2 variation is consistent with the findings of Timmes et al. (1995) for the evolution of $[\text{V}/\text{Fe}]$ as a function of $[\text{Fe}/\text{H}]$.

Chromium (Cr) is predominantly synthesised during incomplete silicon burning in SNe Ia from near-Chandrasekhar mass white dwarfs (Seitenzahl & Townsley 2017) and explosive oxygen and silicon burning more generally (see Côté et al. (2020); Bergemann & Cescutti (2010)). The more neutron-rich isotopes of Cr (such as ^{54}Cr) are produced in high-density Chandrasekhar mass SNe Ia, where electron captures drive the material to be more neutron-rich. This was argued by Bravo et al. (2022) as further support for the idea that the majority of SNe Ia must come from sub-Chandrasekhar (lower density) white dwarfs. Our work shows a rise in the abundance of Cr relative to iron, similar to the behaviour of other Fe-peak elements. More so, more Cr is produced between 5 – 6.5 Gyr as we see a rise in the gradient by a factor of ~ 1.5 compared to the 6.5 – 8 (older) age range.

Manganese (Mn) Type Ia supernovae are an essential nucleosynthesis site for the mono-isotopic manganese (Mn) element. Mn has evolved to a critical element for inferences on the nature of SNe Ia from Galactic Chemical Evolution studies, both in the Milky Way (Seitenzahl et al. 2013; Lach et al. 2020; Eitner et al. 2020, 2023) as well as in Dwarf Galaxies (North et al. 2012; McWilliam et al. 2003, 2018; de los Reyes et al. 2020). The creation of Mn in near-Chandrasekhar mass SNe Ia depends crucially on the entropy during freeze-out from nuclear statistical equilibrium (for reviews see Seitenzahl & Townsley 2017; Seitenzahl & Pakmor 2023). For sub-Chandrasekhar mass models, Mn production occurs chiefly in incomplete silicon burning, where the outcome depends on the metallicity of the explosion (Lach et al. 2020). In this study, we observe a consistent enrichment and a noticeable increase between 5 – 6.5 Gyr (see Fig. 4).

Nickel (Ni) is mostly synthesised by SN Ia explosions with roughly $\sim 1/3$ of the contribution coming from core-collapse supernovae (Woosley & Weaver 1995; Timmes et al. 1995) in both explosive silicon burning and through alpha-rich freeze-out. The

increase in Ni observed for younger stellar populations has also been observed in Feltzing et al. (2009) and Nissen et al. (2020).

Copper (Cu) We see a relatively high copper (Cu) enrichment in the young population of the old sequence from Fig. 4 between 6.3 and 5 Gyr. The overproduction of Cu was first reported by Sneden et al. (1991). Also, according to a study by Bisterzo et al. (2004), the synthesis of Cu in massive stars is attributed to a weak neutron capture process during hydrostatic He-burning and C-burning phases in massive stars. In addition, Weaver & Woosley (1978) and Iwamoto et al. (1999) predict a high abundance of copper at solar metallicity, citing the overproduction of the element due to the metallicity effect from the progenitors of core-collapse SNe (see 4.1). Canonically, it has been predicted that Cu is mostly synthesised through exploding massive stars (Woosley & Weaver 1995). As a result, as we approach higher metallicities, the expectation is that the abundance of Cu should decrease. However, our result shows a significant increase (see Tab. 1). Although Type Ia supernovae are generally not considered to make a substantial contribution to the production of Cu, Lach et al. (2020) found from their theoretical approach that the helium shell detonation model of SNe Ia produces high Cu relative to Fe. Taken together, these findings consequently challenge the existing paradigm for nucleosynthesis of copper.

Zinc (Zn) is synthesised primarily in massive and dying low-mass stars (Nomoto et al. 1997; Mishenina et al. 2002; Nomoto et al. 2013).

Kobayashi et al. (2006) underscores the usefulness of Zn for the study of damped Lyman α systems. We do see a change in the abundance gradient as a function of age around 6.3 Gyr, which is also seen for some other elements around the iron peak (see 4.2.4). Though Zn lies near the Fe-peak, we note from Fig. 3 that it initially exhibits a somewhat flat, slightly decreasing trend, after which we see a rise in its abundance (the elbow effect) around 6.3 Gyr, which is similar to the trend we observe in the α element Mg (and possibly Si).

4.2.5. Others

Both Y and Ba are neutron-capture elements. The gradient of Ba in the younger stellar population of the old sequence shows a decrease in its elemental abundance per Gyr by a factor of 3 compared with the gradient of the entire range of the old sequence.

Yttrium (Y) is a neutron capture element mainly synthesised in AGB stars (Bensby et al. 2017; Kobayashi et al. 2020). At higher temperatures, Y suffers from NLTE effects, i.e., the lines are weakened due to increasing $[\text{Fe}/\text{H}]$ or increasing effective temperature T_{eff} of the stellar model atmosphere (Delgado Mena et al. 2021; Bensby et al. 2014, 2017; Storm & Bergemann 2023). We note that the abundance of Y is well below solar over the old sequence (see Fig. 2) and remains rather flat (though overall rising) over the entire old sequence age range.

Barium (Ba) is another neutron capture element. We find the difference in the gradient between 5-8 Gyr and 5-6.5 Gyr varies by a factor of two. We note the older age range of the old sequence exhibits a rather flat trend (perhaps a slight decrease) up to about 6.3 Gyr (Fig. 3). One could say this particular trend is unique among all elements studied in this work, though alpha element Ca and possibly Ti arguably show a similar trend.

4.2.6. Key findings for age-abundance trends

We found the following overall trends among the element groups:

- Strong, positive enhancement trends for most odd-Z elements (Na, Al, Sc) and most elements near the iron peak (V, Cr, Mn, Ni, Cu, Zn)
- We found a relatively flat abundance trend for alpha-process elements (Mg, Si, Ca, and also Ti)
- We found a decreasing trend for O, as well as C (but less so) on the light side and Ba on the heavy side of the periodic table
- For K, Co and La, our results were inconclusive. We attempted to explain possible reasons for the behaviour exhibited by Y, though we note that Y is one of the elements we analysed that has relatively high uncertainty.

4.3. Implications for nucleosynthesis

The increasing trend of $[(\text{Na}, \text{Al}, \text{Sc})/\text{Fe}]$ differs from what we expect based on their canonically assumed primary nucleosynthetic origins. One potential factor leading to an increasing abundance of Na with decreasing stellar age could be the effect of increasing metallicity on Galactic enrichment from core-collapse supernova explosions (Woosley & Weaver 1994; Kobayashi et al. 2006; Nomoto et al. 2013; Limongi & Chieffi 2018, see 4.1). Another could be asymptotic giant branch (AGB) stars; AGB stars have been proposed as a possible reason for the rising abundance trend at super-solar metallicity (Shi et al. 2004; Kobayashi et al. 2011; Cinquegrana & Karakas 2022).

For most Fe-group elements, the observed rising trend is consistent with predictions for the existing nucleosynthetic paradigm due to the increasingly dominant role of exploding white dwarfs with time (i.e. as we look at younger stars in our Galaxy, we increasingly see the footprint of SN Ia nucleosynthesis). Furthermore, α -elements (i.e., Mg, Si, Ca, and additionally Ti) generally remain flat for the old sequence between $\sim 6.3 - 8$ Gyr, after which there is a gradual decrease (so-called knee; first reported by McWilliam (1997)) in their elemental abundances due to the diminishing contribution of core-collapse SNe and increasing birthrate of SNe Ia. The trend in magnesium (Mg) follows the same age-abundance trend seen in all iron-peak elements in the younger old disc sequence (with a positive gradient), contrary to what we may expect (i.e. that Mg should follow a similar behaviour as other α elements relative to iron and flatten out or become more negative with decreasing age). Also, light elements carbon (C), oxygen (O), and neutron capture elements (Ba and Y) show a decreasing trend towards younger stars.

Of the elements that showed enrichment in their abundances, copper (Cu) upward trend has the highest age-abundance trend, followed by sodium (Na; see Tab. 1). On average, for these elements, more enrichment occurred at 6.3 Gyr by a factor of 3 in their respective gradients. Although copper ($\text{Cu} = 29$) and zinc ($\text{Zn} = 30$) lie close on the periodic table, they have different age-abundance gradient values. Cu and Zn abundance trends are somewhat flat between 8 and 6.3 Gyr. However, Zn quickly rises and remains flat between 6 and 5 Gyr. On the other hand, Cu has a gradual but sustained increase in its abundance from ~ 6 Gyr.

4.4. Putting the old sequence trends into the perspective of the young sequence

While our study focuses on the old sequence of the Milky Way, a similar survey for solar-twin stars was carried for stars of the thin disc out by Spina et al. (2016) to trace the chemical evolution of the Galactic thin disc by examining the $[\text{X}/\text{Fe}]$ versus age for 24 elements from carbon (C) to europium (Eu). Spina et al. (2016) used the high-resolution data and high signal-to-noise UVES optical spectrograph of the VLT spectra of nine solar twins to obtain precise estimates of stellar ages and chemical abundances. The study revealed that each class of elements showed a distinct evolution with time, depending on the different characteristics, rates, and timescales of the nucleosynthesis sites from which they are produced. Findings from the study showed that α -elements (i.e., Ca, Ti, Mg, Si, e.t.c.) are characterised by a $[\text{X}/\text{Fe}]$ decrease with time, while the iron-peak elements (i.e., V, Cr, Mn, Ni, Co, etc.) show an early $[\text{X}/\text{Fe}]$ increase that peaks at around 6 Gyr followed by a decrease towards the youngest stars.

4.5. The significance of an enrichment change at 6.3 Gyr

We appreciate that we have made a seemingly arbitrary cut fitting the age-abundance trends above and below 6.3 Gyr. However, this decision is inspired by previous reports of a knee-age effect by Edvardsson et al. (1993) and McWilliam (1997). After this, several other studies have reported this knee-age effect, mostly seen in α -element plots (Bensby et al. 2014; Spina et al. 2016). The occurrence of the “knee” indicates the onset of the dominant role of (ideally) one nucleosynthesis source relative to another. Various authors have provided different explanations for the presence of the “knee” phenomenon. One view, proposed by McWilliam (1997), suggests that the knee effect indicates varying star formation rates between distinct stellar populations such as the bulge, halo, and Galactic discs. Another view, expressed by Nissen et al. (2020), suggests that the knee can be interpreted as evidence of gas accretion onto the Galactic disc, with a quenching of star formation in between.

This work shows the occurrence of the knee-age effect (or elbow-age effect) in most elements considered around 6.3 Gyr. For odd-Z and Fe-peak elements, we see an upward trend in the $[\text{X}/\text{Fe}]$ beyond the knee – which we have coined an elbow – and for light and alpha-elements, we notice a decreasing trend afterwards (classic knee). For elements near the iron peak, we interpret this trend as the point at which SNe Ia start to make a significant impact on chemical enrichment of the stellar population under study, considering that most of these elements are readily synthesised during SN Ia explosions (Thielemann et al. 2002). Furthermore, we also consider the decreasing trend of alpha and light elements as the point where Type II SNe has reached its peak, consequently leading to a decrease in their $[\text{X}/\text{Fe}]$ as most of these elements are produced through explosions of massive stars (Arnett 1995; Iwamoto et al. 1999; Kobayashi et al. 2011). We conclude by noting that the knee-age effect from this work could be interpreted as a different star formation rate (SFR) taking place between the old and young sequences or possibly different gas accretion onto the younger sequence by the old sequence.

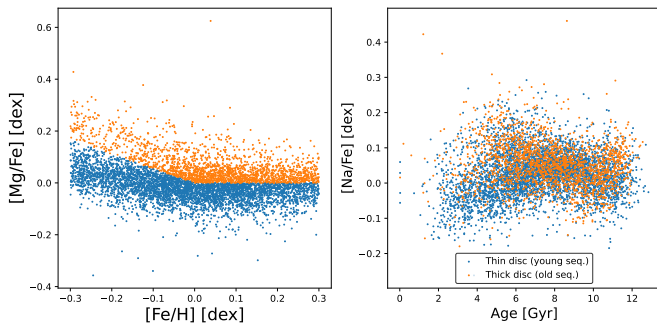


Figure 7. Visualisation of the selection difference of old and young disc stars with the method by Hayden et al. (2017). Panel a) shows the plane of [Fe/H] vs. [Mg/Fe] that was used by Hayden et al. (2017) to select thin and thick disc stars. Panel b) shows that the same stars are less clearly separated in the age-[Na/Fe] we propose in our study. Thick disc stars are orange, while a bluish colour represents the thin disc stars.

4.6. How does our new selection criterion improve the selection of the thick and thin disc stars?

One of our motivations was to try and identify a less contaminated selection method of thin and thick disc stars in the high-metallicity regime, where stars significantly overlap in their dynamics and alpha enhancement. To this end, we have reproduced the linear selection in [Fe/H] vs. [Mg/Fe] used by Hayden et al. (2017) in the [Fe/H] vs [Mg/Fe] plane and we show where these stars are in the Age-[Na/Fe] plane in Fig. 7. To emphasise the point that our selection method is less contaminated, we construct a confusion matrix: the selection criteria of Hayden et al. (2017) is compared against the selection criteria of this work and is presented in Fig. 8. We see that 55% of the stars are attributed to opposite populations. Most notably, Hayden et al. (2017) would allocate 50% (i.e., 3093 stars) of the young sequence as defined in our work as thick disc stars when using [Mg/Fe]. Also, 5% (293 stars) old sequence stars, as described in this work, would be categorised as thin disc stars when using the [Mg/Fe] selection method. In all, only 45% are allocated to the same populations (i.e., 26% thick and 19% thin disc stars). This significant difference in the allocation of stars to the two populations can have critical implications for the study of abundance trends in the Milky Way – most notably the high-metallicity regime, which is more dominant in the inner Galaxy (Matteucci & Francois 1989; Recio-Blanco et al. 2014).

5. Conclusions

In this study, we have presented an analysis of solar-type stars from GALAH DR3 and quantified the abundances of elements at intermediate ages (5-8 Gyr) for solar-type stars (as defined by Nissen et al. 2020). We also presented abundance trends as a function of stellar age for light elements, alpha elements, odd-Z elements, iron peak elements, and neutron capture elements. We offered possible explanations for these elemental abundance trends where feasible. There are two main outcomes of this work:

- Our selection function (Eq. 7) allows us to identify age-abundance trends for the youngest thick disc (young end of the old sequence) stars that are challenging current nucleosynthetic ideas. This is most striking for Na, which shows an increase of 0.0260 ± 0.0009 dex/Gyr for old sequence stars between 5-8 Gyr (see Fig. 4). We also present trends for some elemental abundances (relative to iron) as a function of age (see Tab.

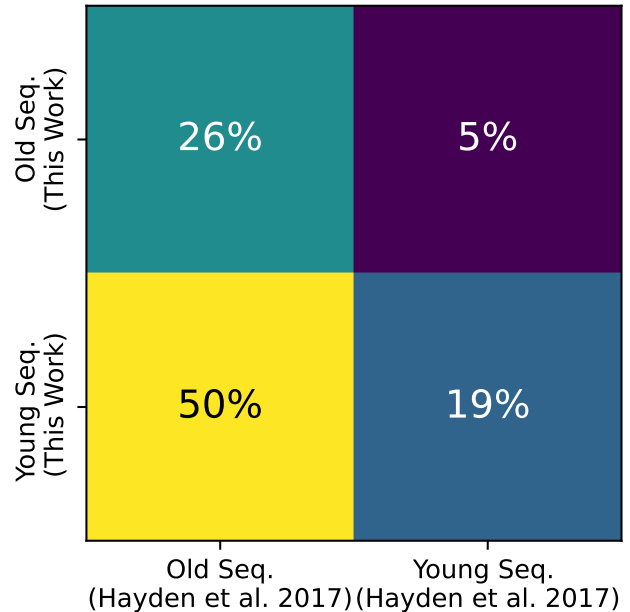


Figure 8. Confusion matrix of the selection of thin and thick disc by Hayden et al. (2017) via low and high [Mg/Fe] (x-axis) and our newly suggested selection method of young and old sequence disc stars via the age-[Na/Fe] plane (y-axis).

- 1) that can be used for improving Galactic chemical evolution models.
- We have shown that at the same age and metallicity, sodium (Na) is a better tracer than [Mg/Fe] vs [Fe/H] to disentangle the old and young sequence disc stars. Our new approach using Na allows us to better separate stars with similar [Fe/H] vs [Mg/Fe] into the old and young sequences, respectively (Fig. 7). Our new selection method using Na improves the false positives by 50% and true negatives by 5%, compared to the [Mg/Fe] vs [Fe/H] approach (see Fig. 8).

In conclusion, we have shown that the different behaviour of Na at intermediate ages is a powerful discriminant to chemically separate the old and young sequence for solar-type stars in the Galactic disc.

Acknowledgements

We acknowledge the traditional owners of the land on which the AAT stands, the Gamilaraay people. We pay our respects to elders past and present and are proud to continue their tradition of surveying the night sky in the Southern Hemisphere. The authors acknowledge fruitful discussions with colleagues, including Alex Kemp, Benoît Côté, Simon Murphy, Giulia Cinquegrana, Philipp Eitner, and Nicholas Storm. This work was supported by the Australian Research Council Centre of Excellence for All Sky Astrophysics in 3 Dimensions (ASTRO 3D) through project number CE170100013. Part of this research was funded through AJR's Australian Research Council Future Fellowship FT170100243 and SB's Australian Research Council DECRA Fellowship DE240100150.

Facilities

AAT with 2df-HERMES at Siding Spring Observatory: The GALAH Survey is based on data acquired through the Australian Astronomical Observatory, under programs: A/2013B/13 (The GALAH pilot survey); A/2014A/25, A/2015A/19, A2017A/18 (The GALAH survey phase 1), A2018 A/18 (Open clusters with HERMES), A2019A/1 (Hierarchical star formation in Ori OB1), A2019A/15 (The GALAH survey phase 2), A/2015B/19, A/2016A/22, A/2016B/10, A/2017B/16, A/2018B/15 (The HERMES-TESS program), and A/2015A/3, A/2015B/1, A/2015B/19, A/2016A/22, A/2016B/12, A/2017A/14, (The HERMES K2-follow-up program). This paper includes data that has been provided by AAO Data Central (datacentral.aao.gov.au). **Gaia:** This work has made use of data from the European Space Agency (ESA) mission *Gaia* (<http://www.cosmos.esa.int/gaia>), processed by the *Gaia* Data Processing and Analysis Consortium (DPAC, <http://www.cosmos.esa.int/web/gaia/dpac/consortium>). Funding for the DPAC has been provided by national institutions, particularly the institutions participating in the *Gaia* Multilateral Agreement. **Other facilities:** This publication makes use of data products from the Two Micron All Sky Survey (Skrutskie et al. 2006) and the CDS VizieR catalogue access tool (Ochsenbein et al. 2000).

Software

The research for this publication was coded in PYTHON (version 3.7.4) and included its packages ASTROPY (v. 3.2.2; Astropy Collaboration et al. 2013, 2018), CORNER (v. 2.0.1; Foreman-Mackey 2016), GALPY (version 1.6.0; Bovy 2015), IPYTHON (v. 7.8.0; Pérez & Granger 2007), MATPLOTLIB (v. 3.1.3; Hunter 2007), NUMPY (v. 1.17.2; Walt et al. 2011), SCIPY (version 1.3.1; Virtanen et al. 2020), We further made use of TOPCAT (version 4.7; Taylor 2005);

Data Availability

The data used for this study is published by Buder et al. (2021) and can be accessed publicly via <https://docs.datacentral.org.au/galah/dr3/overview/>

References

- Alam S., et al., 2015, *ApJS*, **219**, 12
 Amarsi A. M., et al., 2020, *A&A*, **642**, A62
 Anders F., et al., 2014, *A&A*, **564**, A115
 Andrievsky S. M., Spite F., Korotin S. A., François P., Spite M., Bonifacio P., Cayrel R., Hill V., 2011, *A&A*, **530**, A105
 Arnett D., 1995, *ARA&A*, **33**, 115
 Astropy Collaboration et al., 2013, *A&A*, **558**, A33
 Astropy Collaboration et al., 2018, *AJ*, **156**, 123
 Bandyopadhyay A., Thirupathi S., Beers T. C., Susmitha A., 2020, *MNRAS*, **494**, 36
 Bedell M., et al., 2018, *ApJ*, **865**, 68
 Bensby T., Feltzing S., Oey M. S., 2014, *A&A*, **562**, A71
 Bensby T., et al., 2017, *A&A*, **605**, A89
 Bergemann M., Cescutti G., 2010, *A&A*, **522**, A9
 Bisterzo S., Gallino R., Pignatari M., Pompeia L., Cunha K., Smith V., 2004, *Mem. Soc. Astron. Italiana*, **75**, 741
 Bovy J., 2015, *ApJS*, **216**, 29
 Bravo E., Piersanti L., Blondin S., Domínguez I., Straniero O., Cristallo S., 2022, *MNRAS*, **517**, L31
 Buder S., et al., 2018, *MNRAS*, **478**, 4513
 Buder S., et al., 2019, *A&A*, **624**, A19
 Buder S., et al., 2021, *MNRAS*, **506**, 150
 Buder S., et al., 2022, *MNRAS*, **510**, 2407
 Burbidge E. M., Burbidge G. R., Fowler W. A., Hoyle F., 1957, *Reviews of Modern Physics*, **29**, 547
 Cameron A. G. W., 1959, *ApJ*, **130**, 429
 Cayrel R., et al., 2004, *A&A*, **416**, 1117
 Christensen-Dalsgaard J., 2008, *Ap&SS*, **316**, 13
 Cinquegrana G. C., Karakas A. I., 2022, *MNRAS*, **510**, 1557
 Côté B., Jones S., Herwig F., Pignatari M., 2020, *ApJ*, **892**, 57
 Crocker R. M., et al., 2017, *Nature Astronomy*, **1**, 0135
 Das P., Hawkins K., Jofré P., 2020, *MNRAS*, **493**, 5195
 De Silva G. M., et al., 2015, *MNRAS*, **449**, 2604
 Delgado Mena E., Adibekyan V., Santos N. C., Tsantaki M., González Hernández J. I., Sousa S. G., Bertrán de Lis S., 2021, *A&A*, **655**, A99
 Denisenkov P. A., Denisenkova S. N., 1990, *Soviet Astronomy Letters*, **16**, 275
 Edvardsson B., Andersen J., Gustafsson B., Lambert D. L., Nissen P. E., Tomkin J., 1993, *A&A*, **275**, 101
 Eitner P., Bergemann M., Hansen C. J., Cescutti G., Seitzzahl I. R., Larsen S., Plez B., 2020, *A&A*, **635**, A38
 Eitner P., Bergemann M., Ruiter A. J., Avril O., Seitzzahl I. R., Gent M. R., Côté B., 2023, *A&A*, **677**, A151
 El Eid M. F., Champagne A. E., 1995, *ApJ*, **451**, 298
 Feltzing S., Primas F., Johnson R. A., 2009, *A&A*, **493**, 913
 Foreman-Mackey D., 2016, *The Journal of Open Source Software*, **1**, 24
 Gaia Collaboration et al., 2021, *A&A*, **650**, C3
 García R. A., Ballot J., 2019, *Living Reviews in Solar Physics*, **16**, 4
 Gilmore G., Reid N., 1983, *MNRAS*, **202**, 1025
 Griffith E. J., Weinberg D. H., Buder S., Johnson J. A., Johnson J. W., Vincenzo F., 2022, *ApJ*, **931**, 23
 Gustafsson B., Edvardsson B., Eriksson K., Jørgensen U. G., Nordlund Å., Plez B., 2008, *A&A*, **486**, 951
 Hayden M. R., Recio-Blanco A., de Laverny P., Mikolaitis S., Worley C. C., 2017, *A&A*, **608**, L1
 Hunter J. D., 2007, *Comput Sci Eng*, **9**, 90
 Iwamoto K., Brachwitz F., Nomoto K., Kishimoto N., Umeda H., Hix W. R., Thielemann F.-K., 1999, *ApJS*, **125**, 439
 José J., Iliadis C., 2011, *Reports on Progress in Physics*, **74**, 096901
 Karakas A. I., 2010, *MNRAS*, **403**, 1413
 Katz D., Gómez A., Haywood M., Snaith O., Di Matteo P., 2021, *A&A*, **655**, A111
 Kemp A. J., Karakas A. I., Casey A. R., Izzard R. G., Ruiter A. J., Agrawal P., Broekgaarden F. S., Temmink K. D., 2021, *MNRAS*, **504**, 6117
 Kobayashi C., Umeda H., Nomoto K., Tominaga N., Ohkubo T., 2006, *ApJ*, **653**, 1145
 Kobayashi C., Karakas A. I., Umeda H., 2011, *MNRAS*, **414**, 3231
 Kobayashi C., Karakas A. I., Lugaro M., 2020, *ApJ*, **900**, 179
 Kordopatis G., et al., 2013, *AJ*, **146**, 134
 Kromer M., Sim S. A., Fink M., Röpkke F. K., Seitzzahl I. R., Hillebrandt W., 2010, *ApJ*, **719**, 1067
 Kunder A., et al., 2017, *AJ*, **153**, 75
 Lach F., Röpkke F. K., Seitzzahl I. R., Côté B., Gronow S., Ruiter A. J., 2020, *A&A*, **644**, A118
 Lee Y. S., et al., 2011, *ApJ*, **738**, 187
 Limongi M., Chieffi A., 2018, *ApJS*, **237**, 13
 Lindgren L., et al., 2018, *A&A*, **616**, A2
 Lombardo L., et al., 2022, *A&A*, **665**, A10
 Maoz D., Mannucci F., Brandt T. D., 2012, *MNRAS*, **426**, 3282
 Matteucci F., Brocato E., 1990, *ApJ*, **365**, 539
 Matteucci F., Francois P., 1989, *MNRAS*, **239**, 885
 Matteucci F., Greggio L., 1986, *A&A*, **154**, 279
 McWilliam A., 1997, *ARA&A*, **35**, 503
 McWilliam A., 2016, *Publ. Astron. Soc. Australia*, **33**, e040
 McWilliam A., Rich R. M., Smecker-Hane T. A., 2003, *ApJ*, **593**, L145
 McWilliam A., Piro A. L., Badenes C., Bravo E., 2018, *ApJ*, **857**, 97
 Mishenina T. V., Kovtyukh V. V., Soubiran C., Travaglio C., Busso M., 2002, *A&A*, **396**, 189

- Mowlavi N., 1999, *A&A*, **350**, 73
- Nakamura T., Umeda H., Nomoto K., Thielemann F.-K., Burrows A., 1999, *ApJ*, **517**, 193
- Nissen P. E., 2015, *A&A*, **579**, A52
- Nissen P. E., Schuster W. J., 2010, *A&A*, **511**, L10
- Nissen P. E., Christensen-Dalsgaard J., Mosumgaard J. R., Silva Aguirre V., Spitoni E., Verma K., 2020, *A&A*, **640**, A81
- Nomoto K., Iwamoto K., Nakasato N., Thielemann F. K., Brachwitz F., Tsujimoto T., Kubo Y., Kishimoto N., 1997, *Nuclear Phys. A*, **621**, 467
- Nomoto K., Kobayashi C., Tominaga N., 2013, *ARA&A*, **51**, 457
- North P., et al., 2012, *A&A*, **541**, A45
- Ochsenbein F., Bauer P., Marcout J., 2000, *A&AS*, **143**, 23
- Panther F. H., Seitenzahl I. R., Ruiter A. J., Siebert T., Sim S., Crocker R. M., 2021, *MNRAS*, **508**, 1590
- Pérez F., Granger B. E., 2007, *Comput Sci Eng*, **9**, 21
- Peterson R. C., 1981, *ApJ*, **244**, 989
- Piskunov N., Valenti J. A., 2017, *A&A*, **597**, A16
- Prantzos N., Abia C., Limongi M., Chieffi A., Cristallo S., 2018, *MNRAS*, **476**, 3432
- Randich S., Gilmore G., Gaia-ESO Consortium 2013, *The Messenger*, **154**, 47
- Recio-Blanco A., et al., 2014, *A&A*, **567**, A5
- Röpke F. K., et al., 2012, *ApJ*, **750**, L19
- Ruiter A. J., Belczynski K., Fryer C., 2009, *ApJ*, **699**, 2026
- Ruiter A. J., Belczynski K., Sim S. A., Hillebrandt W., Fryer C. L., Fink M., Kromer M., 2011, *MNRAS*, **417**, 408
- Salpeter E. E., 1952, *ApJ*, **115**, 326
- Seitenzahl I. R., Pakmor R., 2023, *Handbook of Nuclear Physics*, pp 3809–3842
- Seitenzahl I. R., Townsley D. M., 2017, in Alsabti A. W., Murdin P., eds, *Handbook of Supernovae*. Springer, Cham, p. 1955, doi:10.1007/978-3-319-21846-5_87
- Seitenzahl I. R., Cescutti G., Röpke F. K., Ruiter A. J., Pakmor R., 2013, *A&A*, **559**, L5
- Sharma S., et al., 2018, *MNRAS*, **473**, 2004
- Sheinis A., et al., 2015, *Journal of Astronomical Telescopes, Instruments, and Systems*, **1**, 035002
- Shi J. R., Gehren T., Zhao G., 2004, *A&A*, **423**, 683
- Siess L., 2006, *A&A*, **448**, 717
- Skrutskie M. F., et al., 2006, *AJ*, **131**, 1163
- Smiljanic R., et al., 2016, *A&A*, **589**, A115
- Snedden C., Gratton R. G., Crocker D. A., 1991, *A&A*, **246**, 354
- Soderblom D. R., King J. R., 1998, in Hall J. C., ed., *Solar Analogs: Characteristics and Optimum Candidates*. p. 41
- Spina L., Meléndez J., Karakas A. I., Ramírez I., Monroe T. R., Asplund M., Yong D., 2016, *A&A*, **593**, A125
- Spina L., et al., 2018, *MNRAS*, **474**, 2580
- Storm N., Bergemann M., 2023, *MNRAS*, **525**, 3718
- Taylor M. B., 2005, in Shopbell P., Britton M., Ebert R., eds, *Astronomical Society of the Pacific Conference Series Vol. 347, Astronomical Data Analysis Software and Systems XIV*. p. 29
- Thielemann F. K., et al., 2002, *Ap&SS*, **281**, 25
- Timmes F. X., Woosley S. E., Weaver T. A., 1995, *ApJS*, **98**, 617
- Tur C., Heger A., Austin S. M., 2010, *arXiv e-prints*, p. arXiv:1012.4732
- Valenti J. A., Piskunov N., 1996, *A&AS*, **118**, 595
- Virtanen P., et al., 2020, *Nature Methods*, **17**, 261
- Walt S. v. d., Colbert S. C., Varoquaux G., 2011, *Comput Sci Eng*, **13**, 22
- Weaver T. A., Woosley S. E., 1978, *Evolution and explosion of massive stars*, Presented at the 13th Texas Symp. on Relativistic Astrophys., Munich, 14–19 Dec. 1979
- Woosley S. E., 1986, in Audouze J., Chiosi C., Woosley S. E., eds, *Saas-Fee Advanced Course 16: Nucleosynthesis and Chemical Evolution*. p. 1
- Woosley S. E., Weaver T. A., 1994, *ApJ*, **423**, 371
- Woosley S. E., Weaver T. A., 1995, *ApJS*, **101**, 181
- Yanny B., et al., 2009, *AJ*, **137**, 4377
- Yoshii Y., 1982, *PASJ*, **34**, 365
- Zhao G., Zhao Y.-H., Chu Y.-Q., Jing Y.-P., Deng L.-C., 2012, *Research in Astronomy and Astrophysics*, **12**, 723
- da Silva R., Porto de Mello G. F., Milone A. C., da Silva L., Ribeiro L. S., Rocha-Pinto H. J., 2012, *A&A*, **542**, A84
- de los Reyes M. A. C., Kirby E. N., Seitenzahl I. R., Shen K. J., 2020, *ApJ*, **891**, 85